THEORETICAL STUDIES ON THE ELECTRICAL ACTIVITY OF PANCREATIC β-CELLS AS A FUNCTION OF GLUCOSE

DANIEL MARC HIMMEL AND TERESA REE CHAY
Department of Biological Sciences, University of Pittsburgh, Pittsburgh, Pennsylvania 15260

ABSTRACT The electrical activity of pancreatic β-cells, which has been closely correlated both with intracellular Ca^{2+} concentration and insulin release, is characterized by a biphasic response to glucose and bursts of spiking action potentials. Recent voltage clamp and single channel patch clamp experiments have identified several transmembrane ionic channels that may play key roles in the electrophysiological behavior of β-cells. There is a hypothesis that Ca^{2+}-activated K^+ channels are responsible for both the resting potential during low glucose concentration and the silent phase during bursting. The discovery of the ATP-inactivated K^+ channel raises the possibility that the current for this latter K^+ channel may dominate the resting potential, while the Ca^{2+}-activated K^+ current dominates the silent phase potential between bursts. The recent discovery that Ca^{2+}-activated K^+ channels are pH sensitive raises an interesting possibility for the biphasic electrical response. In this paper, numerical methods are presented for evaluating these hypotheses against experimental evidence.

INTRODUCTION

Pancreatic β-cells in the islets of Langerhans exhibit a characteristic electrical activity on their plasma membranes that is greatly influenced by glucose concentration in the perfusion medium. The electrical activity typically has several characteristics. During low glucose concentration, the membrane potential is at the resting potential of ~ −70 mV. If an intermediate glucose concentration is then introduced, the β-cells exhibit what is referred to as a biphasic response. In the first phase (i.e., transient phase) of this response, the potential climbs to a plateau potential at ~ −36 mV and remains there for 2–3 min (in this paper, an increase in potential denotes a change in the positive direction). Superimposed on this plateau potential are rapid action potential spikes. The plateau potential ends with a repolarization to ~ −45 mV. The plasma membrane remains there for ~30 s–1 min before it rises again to the plateau potential. The plateau potential with superimposed spikes is commonly referred to as a "burst." The spikes of a burst oscillate between −36 mV and −20 mV. When the plasma membrane repolarizes to below −45 mV after a burst, it is said to enter the "silent phase." When spiking is occurring (e.g., in a burst), the cell is said to be in the "active phase" (4, 7, 29). In the next several minutes after the transient phase, short repetitive bursts occur and gradually stabilize to a "limit cycle" (usually described by electrophysiologists as the "steady-state"), in which bursts separated by silent phases (with the minimum potential between −50 mV and −55 mV) occur at a regular interval. Here, all bursts will have the same duration and frequency. This second phase will continue for as long as glucose remains at the elevated level (4, 7, 29).

The duration of bursts in the limit cycle is a function of glucose concentration. Thus, the percent of total time occupied by the active phase (percent relative active duration, or %RAD) is related to glucose concentration in a sigmoidal fashion. At high glucose concentrations, bursting is replaced by continuous spiking (%RAD = 100%) (4, 29, 30). Moreover, the spike frequency (spikes per second) is also related to glucose concentration roughly in a sigmoidal fashion (36).

Current experimental evidence strongly favors the view that this electrical activity is closely correlated with the regulation of insulin secretion (1, 6, 29, 30, 33, 36, 38). It is generally believed that insulin exocytosis from β-cells is potentiated by a transient increase in free intracellular calcium cations (for a review, see reference 37). Rorsman et al. (34) have shown that when a high glucose concentration is introduced, intracellular free Ca^{2+} concentration ($[Ca^{2+}]_i$) rises. However, in the presence of D-600, a blocker of voltage-sensitive calcium channels, $[Ca^{2+}]_i$ drops for ~1–3 min, indicating that intracellular sequestration of Ca^{2+} may be occurring and that this sequestration is masked by an influx of extracellular Ca^{2+} through voltage-sensitive channels in the plasma membrane. These views are supported by work done by Herchuelz and Malaisse (24). They report that, in response to glucose stimulation. $^{45}Ca^{2+}$ efflux drops for 3–4 min and then increases dramat-

Correspondences should be sent to Dr. Teresa Ree Chay at the above address.

ically. The secondary rise in efflux of $^{45}Ca^{2+}$ occurs only in the presence of extracellular Ca^{2+}. Thus, Herchuelz and Malaisse contend that the secondary rise in efflux reflects an increase in $[Ca^{2+}]_i$ from influx of extracellular Ca^{2+}. The findings of Rorsman et al. and Herchuelz and Malaisse strongly support the notion that Ca^{2+} is sequestered intracellularly during the transient phase, because the drop in $[Ca^{2+}]_i$ is accompanied by a drop, not a rise, in Ca^{2+} efflux (24, 34). As will be seen, intracellular calcium plays a major role in the electrophysiological activity of pancreatic β-cells.

In the early 1980's, it was widely believed that three transmembrane ionic channels play key roles in β-cell electrical activity. These were (*a*) a voltage-gated Ca^{2+} channel (23, 37), (*b*) a voltage-gated K^+ channel (5, 21, 22), and (*c*) a Ca^{2+}-activated K^+ channel (2, 3). However, recent patch clamp work (15, 17, 18), indicating that the voltage-gated K^+ channel is sensitive to $[Ca^{2+}]_i$, has cast doubt on the existence of a separate Ca^{2+}-activated K^+ channel (for a brief review of Ca^{2+}-activated K^+ channels in various organisms, see Petersen and Maruyana [32]). During patch clamp experiments, Cook et al. [15] reported a pH dependence for the Ca^{2+}-activated voltage-gated K^+ channel in neonatal rat pancreatic β-cells. Meanwhile, other patch clamp work has established the presence of an ATP-inhibited K^+ channel (1, 14).

Based on experimental evidence, Atwater et al. (3, 4) proposed that a Ca^{2+}-activated K^+ channel was responsible for both the resting potential and the silent phase during bursting. They suggested that the sensitivity of initial electrical activity to a threshold glucose concentration was attributable to this current. They also suggested that glucose enhances sequestration efflux of intracellular Ca^{2+} (Ca_i) by activating various energy requiring processes, such as mitochondrial sequestration and the Ca^{2+}-ATPase pump activity in the plasma membrane. Thus, according to their hypothesis, the glucose dependence of the electrical activity owes its origin to the rate of efflux and intracellular sequestration of Ca_i. The hypothesis of Atwater et al. (3, 4) has been mathematically modelled by Chay and Keizer (11). Numerical simulations of the model are in good agreement with experimental measurements of the voltage oscillations and predict, as well, oscillations in the intracellular Ca^{2+} concentration (11) and in the intercellular K^+ concentration (12).

Recently, a barrier kinetic model containing the ATP-inactivated K^+ channel has been simulated by Chay (9). In the model by Chay (9), it was assumed that the ATP-inactivated K^+ channel was responsible for the resting potential and that the glucose dependence of the burst activity could be traced to an inhibition of the ATP-inactivated K^+ channel activity by glucose. The sequestration of Ca_i was attributed to the Ca^{2+}-ATPase pump activity, and the efflux rate of Ca_i was taken to be independent of the glucose concentration due to saturating ATP concentrations in the bursting domain. Numerical simulations of the membrane electrical activity gave essentially the same oscillatory pattern as that of Chay and Keizer (11).

In the simulations presented here, a set of potentially useful numerical techniques will be presented to test the efficacy of prevalent mathematical models against experimental evidence. The strengths and shortcomings of our model, with and without the ATP-inhibited K^+ channel, will be examined using these numerical methods. The hypothesis proposed by Atwater et al. (4) will be compared to that by Chay (9) by obtaining experimentally measurable parameters, such as the glucose dose–response of K^+ flux. Additionally, the pH dependence of the Ca^{2+}-activated K^+ channel will be simulated in the absence of the ATP-inactivated K^+ channel. The relevance of these results to the recently discovered Ca_i-sensitive voltage-gated K^+ channel will be discussed along with gaps in our understanding of the background leak currents.

THE SIMULATION MODEL

For our simulations, we use a circuit model equivalent to that of Chay and Keizer (11), but we add an additional current to account for the ATP-inactivated K^+ channel. Unlike the model of Chay and Keizer (11, 12), however, we do not make the assumption that the reversal potential, V_{Ca}, of Ca^{2+} ions is constant. We let the Ca^{2+} reversal potential take the Nernst form (given in Eq. A12 in Appendix A), such that it is a function of the intracellular calcium concentration. One consequence of this is that the amplitude of periodic $[Ca^{2+}]_i$ fluctuations is smaller and in better agreement with experimental findings. As a side effect of making V_{Ca} variable, deterministic chaos becomes possible. Deterministic chaos, in this case, is a situation in which the oscillatory solutions to the differential equations become unstable, so that the burst duration and frequency cannot be uniquely defined. The actual duration and frequency of bursts becomes dependent on initial boundary conditions used in the simulations (e.g., initial voltage, initial $[Ca^{2+}]_i$) in an unpredictable manner (8, 13).

Another difference between our present model and the former one by Chay and Keizer (11, 12) is that we let ℓ in Eq. A5 equal 3 instead of 4 (see Appendix B) and we make $\bar{g}_{K,v}$ smaller. That this change does not lead to any appreciable changes in the resting simulations demonstrates that this parameter is by no means of crucial importance, and it may be properly adjusted as detailed experimental data on $I_{K,v}$ becomes available.

Four ionic currents are represented in the model used here. These are the K^+ current, which consists of a calcium-dependent component ($I_{K,Ca}$), and a voltage-gated component ($I_{K,V}$), the ATP-inactivated K^+ current ($I_{K,ATP}$), the voltage-gated Ca^{2+} current ($I_{Ca,V}$), and the ionic leak current (I_ℓ).

The current model contains three ordinary differential equations: (*a*) the membrane potential (Eq. A11 in Appen-

dix A), which is expressed as a sum of ionic currents carried by outward-going K^+ ions, inward-going Ca^{2+} ions, and the leak current; (*b*) the intracellular Ca^{2+} concentration (Eq. A1 in Appendix A); and (*c*) the probability, n, of opening the voltage-dependent Hodgkin–Huxley gate in the voltage-gated K^+ channel (Eq. A6 in Appendix A). All the equations are given in Appendix A.

METHODS

Simulations were run via a FORTRAN program on a DEC 1022 computer. The three differential equations were solved numerically using a GEAR algorithm (25). The magnitude of the absolute and relative error tolerances required for integration was set at 10^{-7}.

The results of each dynamic simulation were stored in a FORTRAN data file for later analysis. Another FORTRAN program read off time, membrane potential, $[Ca^{2+}]_i$, and the currents, and then calculated mean $[Ca^{2+}]_i$, the mean ionic fluxes, burst frequency, spike frequency, absolute active duration (AAD), and %RAD. Each of these were defined as follows:

(*a*) Mean Ca^{2+} concentration was the average calcium concentration over one complete cycle from the beginning of one burst to the beginning of the next:

$$[Ca^{2+}]_{i,av} = \frac{1}{\tau}\int_0^{\tau}[Ca^{2+}]_i dt,$$

where $[Ca^{2+}]_{i,av}$ is the mean intracellular Ca^{2+} concentration, τ is the period (seconds) from the beginning of one burst to the beginning of the next, and $[Ca^{2+}]_i$ is the intracellular Ca^{2+} concentration at time t. During continuous spiking, mean intracellular calcium concentration was taken as the integral of intracellular calcium concentration over a 1-min interval after stabilization of the simulation. When deterministic chaos occurred, $[Ca^{2+}]_{i,av}$ was calculated for five or more separate burst periods (cycles). These were then averaged together.

(*b*) Mean ionic flux gave the mean flux of ion i over one complete cycle:

$$J_{i,av} = \frac{1}{\tau}\int_0^{\tau}J_i dt,$$

where $J_{i,av}$ is the mean ionic flux of ion i, J_i is the ionic flux at time t of ion i, and i can be either Ca^{2+} (net, influx, or efflux) or K^+ (voltage-gated, calcium-activated, or ATP-inactivated). Again, mean ionic flux during continuous spiking was determined for a 1-min interval after stabilization of the simulation. When deterministic chaos occurred, $J_{i,av}$ was calculated for five or more separate burst periods (cycles). These were then averaged together.

(*c*) Burst frequency was defined as the number of bursts per minute. It was calculated as one burst divided by the time of one burst cycle, τ:

$$\text{Burst frequency} = \frac{1}{\tau}.$$

When deterministic chaos occurred, burst frequency was calculated for five or more separate burst periods (cycles). These were then averaged together.

(*d*) Spike frequency was defined as the number of spikes occurring over one burst cycle divided by the time, τ, in that cycle:

$$\text{Spike frequency} = \frac{\text{No. of spikes}}{\tau}.$$

During continuous spiking, as above, we let τ be 1 min. When deterministic chaos occurred, spike frequency was calculated for five or more separate burst periods (cycles). These were then averaged together.

(*e*) AAD was defined as the burst duration (time from the beginning of a burst to the end of the burst). For non-chaotic activity, every burst in the simulation had the same duration. During deterministic chaos, burst duration tended to be variable. Thus, the equation used to calculate AAD (below) became a mean. When chaos occurred, we ran the simulation as long as practical (2–3 min) to obtain as accurate a value as possible for AAD, but accuracy was nevertheless sacrificed due to the unpredictable nature of deterministic chaos:

$$\text{AAD} = \frac{\text{Total active time}}{\text{No. of bursts}}.$$

During continuous spiking, AAD, by definition, tended toward infinity.

(*f*) %RAD provided a measure of the fraction of total time that was occupied by the active phase (i.e., spiking). Thus, continous spiking gave a value of 100% for %RAD. It was calculated as the duration of a burst divided by the cycle length, τ. During chaos, it was necessary to include several cycles to arrive at a more accurate value. Thus,

$$\%\text{RAD} = \frac{\text{Total active time}}{\text{Total time}} \times 100\%,$$

where "total time" is a time interval calculated as the sum of several burst cycle lengths and "total active time" is the sum of the durations of the bursts occurring in that time interval.

The program detected the onset of a burst when membrane voltage was greater (more positive) than -40 mV and dV/dt was positive. Likewise, the end of a burst was detected when voltage was less (more negative) than -40 mV and dV/dt was negative. Integrals were calculated using the trapezoidal rule and a time increment of 20 ms.

RESULTS

Case I: Effect of Glucose on Calcium Sequestration

To simulate the hypothesis proposed by Atwater et al. (3, 4), $g_{K,ATP}$ was set equal to zero, so that there was no ATP-inactivated K^+ current. Simulations were run for different values of k_{Ca} ranging from 0.0005 to 0.1 ms^{-1} to find the upper and lower limits within which spiking occurred. The lowest value of k_{Ca} for which spiking was found to occur was 0.010. Continuous spiking (not interrupted by bursting activity) was found to occur for $k_{Ca} \geq 0.0435$. Simulations were analyzed for various values of k_{Ca} ranging from 0.0005 to 0.045.

Fig. 1 shows dynamic plots of voltage and $[Ca^{2+}]_i$ versus time for four different values of k_{Ca}. k_{Ca} is printed on the upper-right-hand corner of each plot and is expressed in reciprocal milliseconds (ms^{-1}). The solid line represents membrane potential in millivolts (mV), and the dashed line represents $[Ca^{2+}]_i$ in micromolar (μM). The burst duration increases as k_{Ca} increases. The last plot shows bursts of variable (chaotic), long duration which occur just before k_{Ca} is raised high enough to permit continuous spiking.

One notable characteristic of these plots is that maximum and minimum $[Ca^{2+}]_i$ remain fixed for all values of k_{Ca}. The rate constant k_{Ca} determines how rapidly $[Ca^{2+}]_i$ returns to its minimum value after a burst has occurred. For high values of k_{Ca}, the silent phase between bursts is brief, because $[Ca^{2+}]_i$ rapidly falls to levels for which the

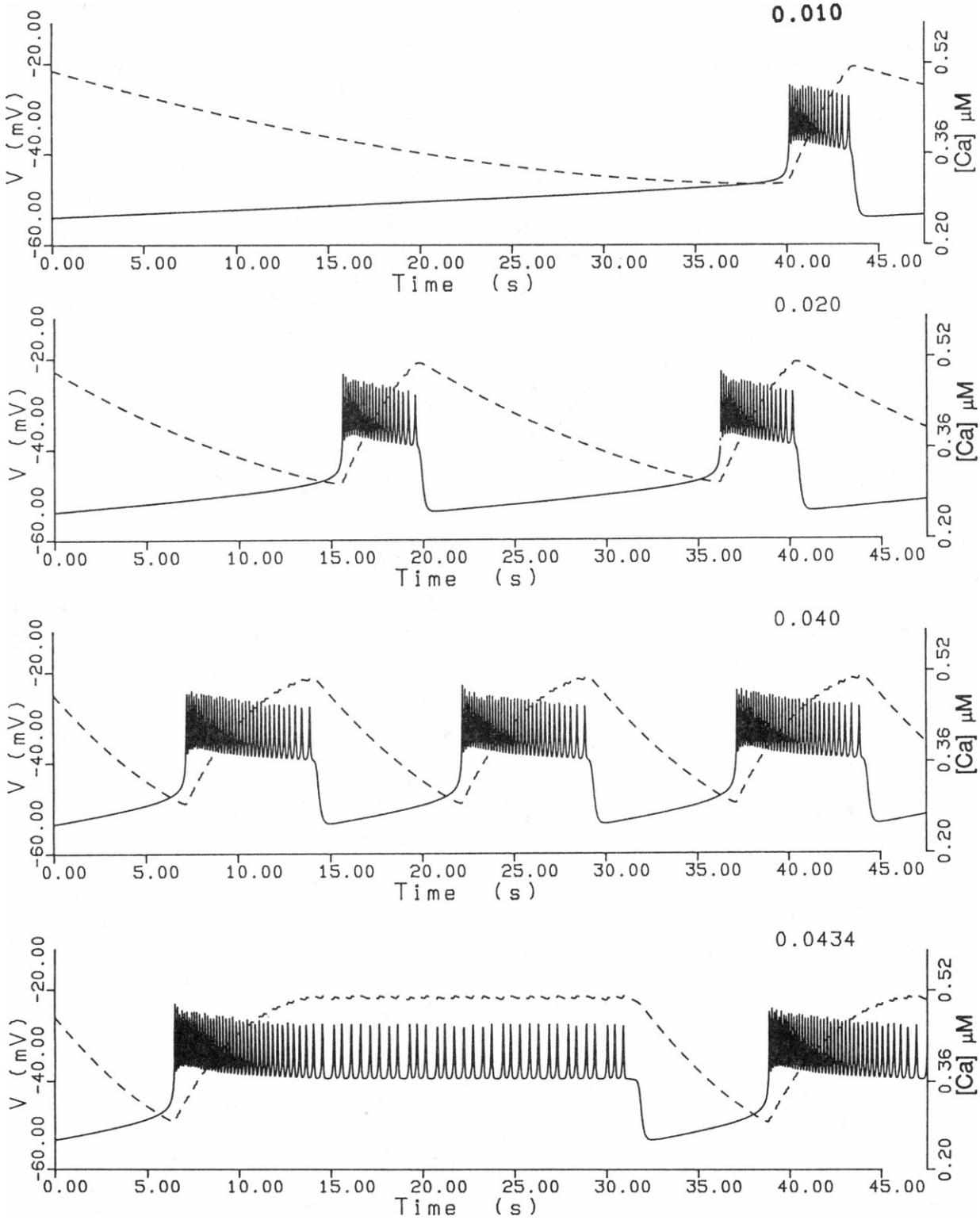

FIGURE 1 Potential vs. time for various values of k_{Ca}. For each trace, the value of k_{Ca} is in the upper-right-hand corner, expressed as ms^{-1}. Superimposed on the time course of membrane potential (mV, *solid line*) is the time course of intracellular calcium concentration (μM, *dashed line*). Time is in seconds.

Ca^{2+}-activated K^+ channel is almost completely inactivated.

It is assumed that k_{Ca} increases as glucose concentration increases. We assume that the glucose dependence of k_{Ca} follows the Hill equation (16). By solving for glucose concentration and taking the logarithm of the quantity $k_{Ca}/(k^*_{Ca} - k_{Ca})$, where k^*_{Ca} is the efflux rate constant at which glucose no longer influences the rate, we avoid having to make any speculative assumptions about the cooperativity (the Hill coefficient) or the binding constant for glucose dissociation from the Ca_i sequestrating receptor molecules. Thus, increasing log glucose concentration is proportional to log $[k_{Ca}/(k^*_{Ca} - k_{Ca})]$. For our purposes, we let $k^*_{Ca} = 0.045$ ms^{-1}, since this value is in the interval for which continuous spiking occurs. Bear in mind that k^*_{Ca} does not appear in the equations of our model and therefore is not a critical parameter.

Fig. 2 depicts four dose–response curves, predicted by Case I, for the β-cell over the k_{Ca} interval tested. Four plots are shown with respect to log $[k_{Ca}/(k^*_{Ca} - k_{Ca})]$. These are %RAD, AAD, spike frequency, and burst frequency. The %RAD gives a roughly sigmoidal curve, although for low x-axis values the curve becomes concave-down. Continuous spiking is designated where %RAD equals 100%. The AAD increases sharply at the onset of electrical activity, increases more slowly during most of the bursting interval, and rapidly approaches infinity near the onset of continuous spiking. The number of spikes per second increases sharply from 0.0 to ~2.4, and forms a concave-down curve during bursting. At the onset of continuous spiking, it decreases somewhat and then levels off near 2.0 spikes/s. Burst frequency forms a concave-down curve and reaches a maximum of about four bursts per minute. In all four plots, small regions of unpredictable fluctuations near the onset of continuous spiking are the result of deterministic chaos.

The mean $[Ca^{2+}]_i$ (see Fig. 3) starts at almost 0.5 μM for $k_{Ca} = 0.0005$ and steadily drops to 0.32 μM at $k_{Ca} = 0.008$ ms^{-1}. Electrical activity begins at $k_{Ca} = 0.01$ ms^{-1}. At this point, $[Ca^{2+}]_i$ jumps abruptly to 0.38 μM and continues to increase very slowly with increasing k_{Ca}. Chaos is observed in electrical activity for values of k_{Ca} just before continuous spiking occurs. In the interval of k_{Ca} for which chaos occurs, $[Ca^{2+}]_i$ fluctuates up and down unpredictably. For $k_{Ca} \geq 0.0436$, continuous spiking occurs. At the beginning of this interval, $[Ca^{2+}]_i$ jumps abruptly from ~0.41 μM to 0.51 μM and levels off at this value for the rest of the interval. Calcium influx through voltage-gated Ca^{2+} channel is almost completely offset by Ca^{2+} efflux.

The total K^+ flux gives a simpler curve (see Fig. 4) with

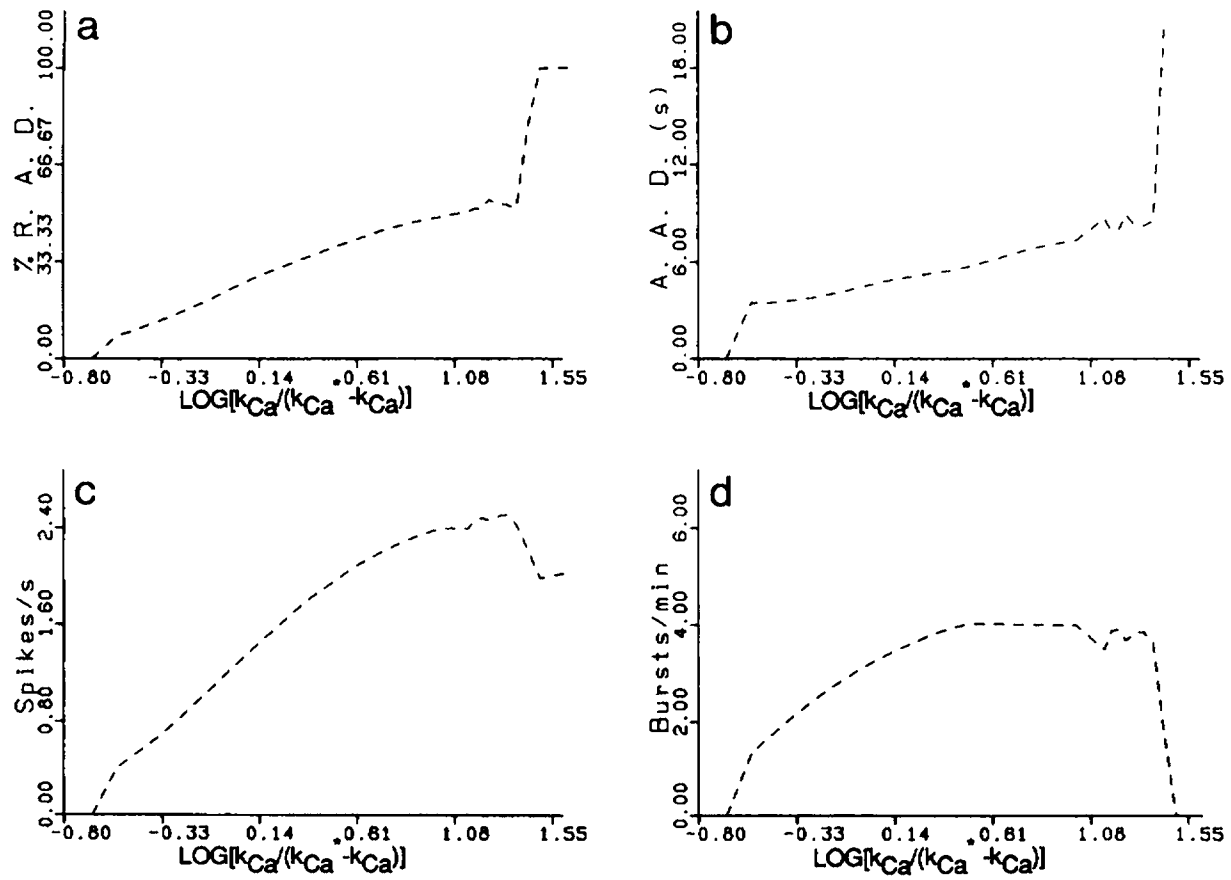

FIGURE 2 Effect of the Ca_i sequestration rate on various dose response curves. The ordinate is log $[k_{Ca}/(k^*_{Ca} - k_{Ca})]$. Shown are (*a*) %RAD, (*b*) AAD (s), (*c*) spike frequency (s^{-1}), and (*d*) burst frequency (min^{-1}). k^*_{Ca} was taken to be 0.045 ms^{-1}.

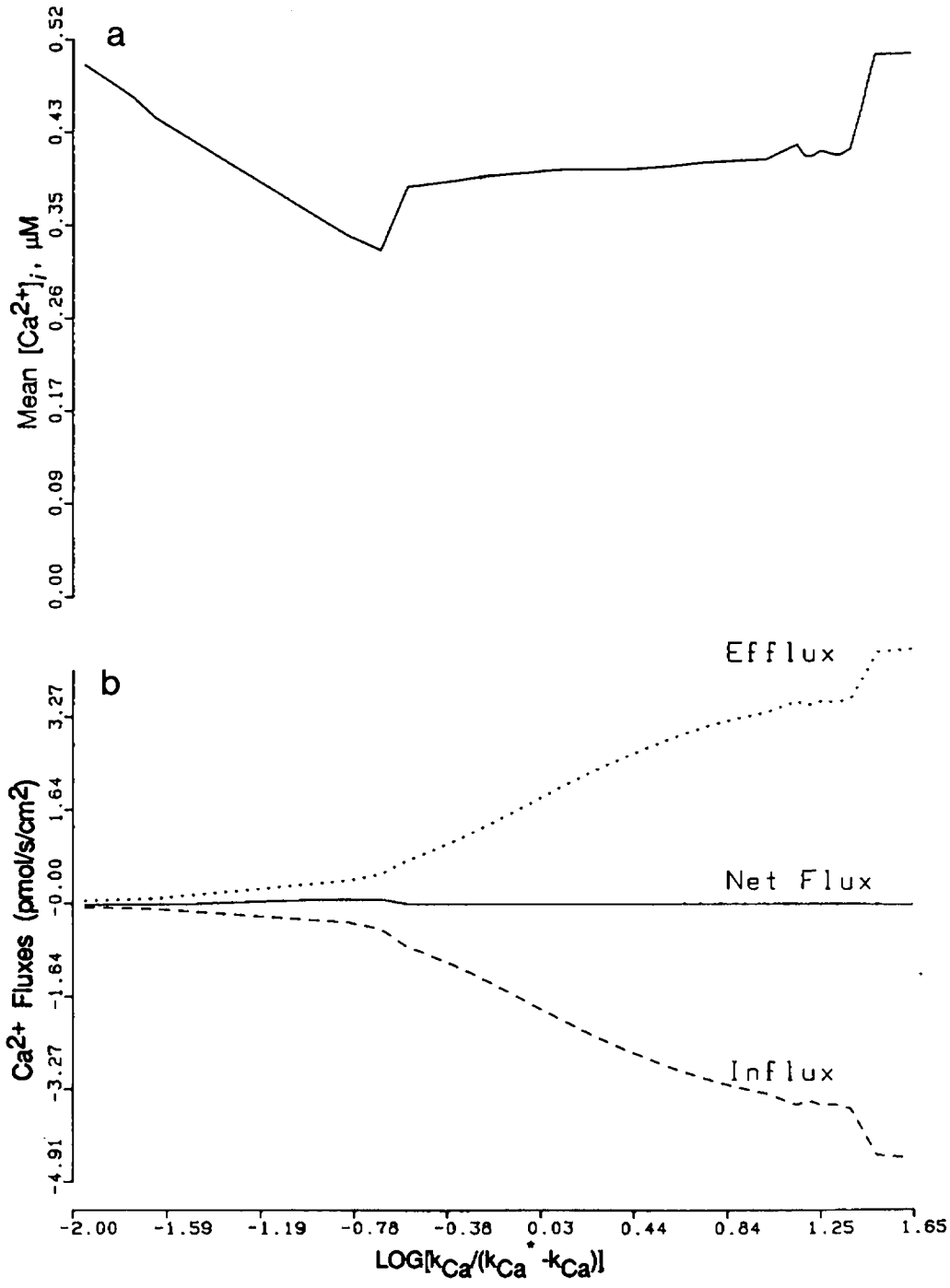

FIGURE 3 Effect of the Ca_i sequestration rate on (*a*) mean intracellular Ca^{2+} concentration (μM) and (*b*) Ca^{2+} fluxes (pmol/s per cm^2). The ordinate is log $[k_{Ca}/(k^*_{Ca} - k_{Ca})]$. (*b*) *Dotted line*, efflux; *dashed line*, influx; *solid line*, net flux.

respect to increasing glucose (increasing k_{Ca}). It remains almost level at 0.95 pmol/s per cm^2 from k_{Ca} = 0.0005 ms^{-1} to k_{Ca} = 0.01 ms^{-1}, where electrical activity begins. During the x-axis interval for which bursting occurs, the total K^+ flux increases substantially in a concave-down fashion, levelling off at 3.6 pmol/s per cm^2. However, an abrupt increase to ~4.3 pmol/s per cm^2 then occurs at the onset of continuous spiking, forming a quasi-sigmoidal tail for large k_{Ca} values.

Case II: Effect of Glucose on the ATP-inactivated K^+ Channel

For these simulations, k_{Ca} was set equal to 0.0450, for which continuous spiking occurred in Case I. Simulations

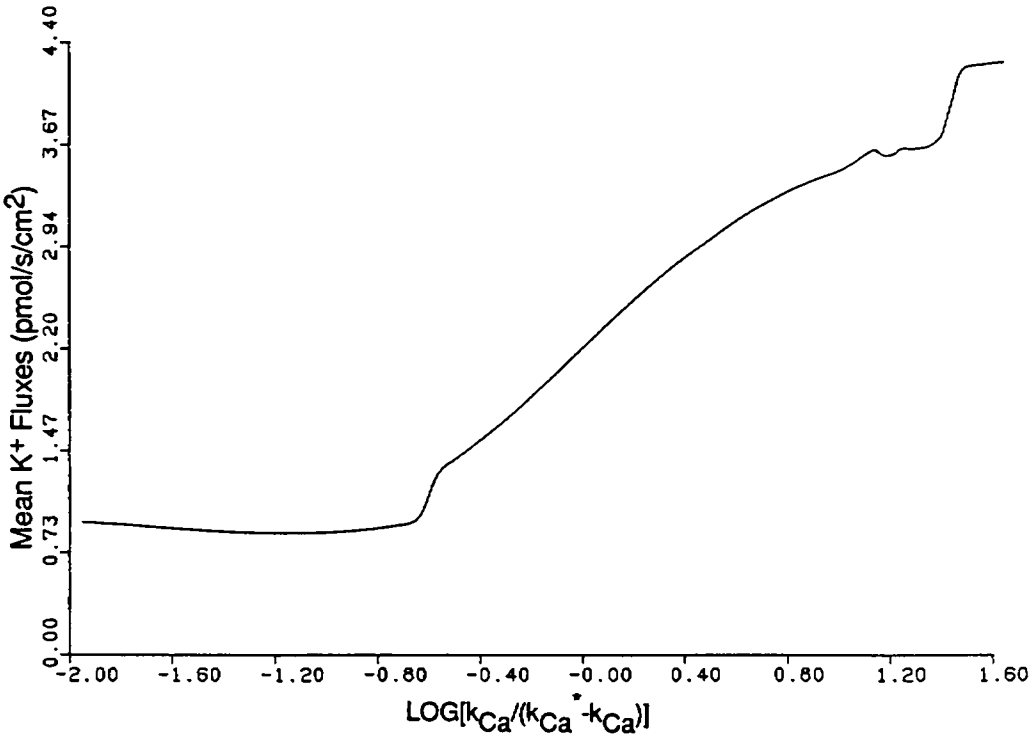

FIGURE 4 Effect of the sequestration rate on K^+ efflux. The ordinate is log $[k_{Ca}/(k^*_{Ca} - k_{Ca})]$. Fluxes are in pmol/s per cm^2.

were run for values of $g_{K,ATP}$ ranging from 7,500 pS to 0 pS. It was found that for very large values of $g_{K,ATP}$, the resting potential became hyperpolarized well below the resting potential of −69 mV to the neighborhood of −85 mV, reducing the driving force for K^+ flux. This hyperpolarization, we believe, was a consequence of our not including rectification in the equation for I_f (more in Discussion). Thus, in the plots presented for this section, we include results for $g_{K,ATP} \leq 100$ pS, where this problem becomes negligible. All electrical activity (i.e., bursting and spiking) occurs for $g_{K,ATP}$ substantially <50 pS.

It is assumed that $g_{K,ATP}$ decreases as glucose concentration increases, and that ATP inhibits the ATP-inactivated K^+ channel noncompetitively. As in Case I, to avoid assumptions about the exact kinetics of the inhibition, we assume that the logarithm of glucose concentration is proportional to log $[(g^*_{K,ATP} - g_{K,ATP})/g_{K,ATP}]$, where $g^*_{K,ATP}$ is the total conductance for the ATP-inactivated K^+ channel in the absence of glucose. In the plots of this section, this relationship will be used to relate $g_{K,ATP}$ to glucose concentration. We use a value of 7,500 pS for $g^*_{K,ATP}$. It is important to bear in mind that $g^*_{K,ATP}$ does not appear in the equations of our model. The choice for this parameter is not crucial, for it does not affect the results reported here.

Fig. 5 shows dynamic plots of voltage and $[Ca^{2+}]_i$ versus time for four different values of $g_{K,ATP}$. $g_{K,ATP}$ is printed on the upper-right-hand corner of each plot and is expressed in picoSiemens (pS). The solid line represents membrane potential (mV) and the dashed line, $[Ca^{2+}]_i$ (in μM). Clearly, as the conductance, $g_{K,ATP}$, through the ATP-inactivated K^+ channels decreases, the active phase gets longer and longer compared to the silent phase. In the last two plots, deterministic chaos is easily noticeable, as the burst duration is variable.

Unlike simulations for Case I, in these simulations the maximum and minimum $[Ca^{2+}]_i$ are not fixed. As $g_{K,ATP}$ decreases, the maximum $[Ca^{2+}]_i$, minimum $[Ca^{2+}]_i$, and the amplitude of the periodic fluctuation in $[Ca^{2+}]_i$ all increase. As $g_{K,ATP}$ gets smaller and smaller, more and more current through the $[Ca^{2+}]_i$-activated K^+ channel is needed to repolarize the membrane enough to terminate a burst. Hence, $[Ca^{2+}]_i$ must climb to a higher maximum before a burst ends. Conversely, as $g_{K,ATP}$ increases, less and less intracellular Ca^{2+} is needed to activate the Ca^{2+}-activated K^+ channel enough to terminate a burst.

Fig. 6 depicts four dose–response curves predicted by Case II over the $g_{K,ATP}$ interval tested. The four plots shown with respect to log $[(g^*_{K,ATP} - g_{K,ATP})/g_{K,ATP}]$ are %RAD, AAD, spikes per second, and bursts per minute. All four curves have the same general shape and characteristics as their counterparts in Case I (Fig. 2).

The mean $[Ca^{2+}]_i$ curve (Fig. 7) differs markedly from that of Case I. It starts at zero, follows a roughly sigmoidal curve which is concave-down over the region for which bursting occurs, and then jumps sharply from 0.430 μM at the onset of continuous spiking and levels off.

Fig. 8 depicts the K^+ fluxes over the domain of $g_{K,ATP}$

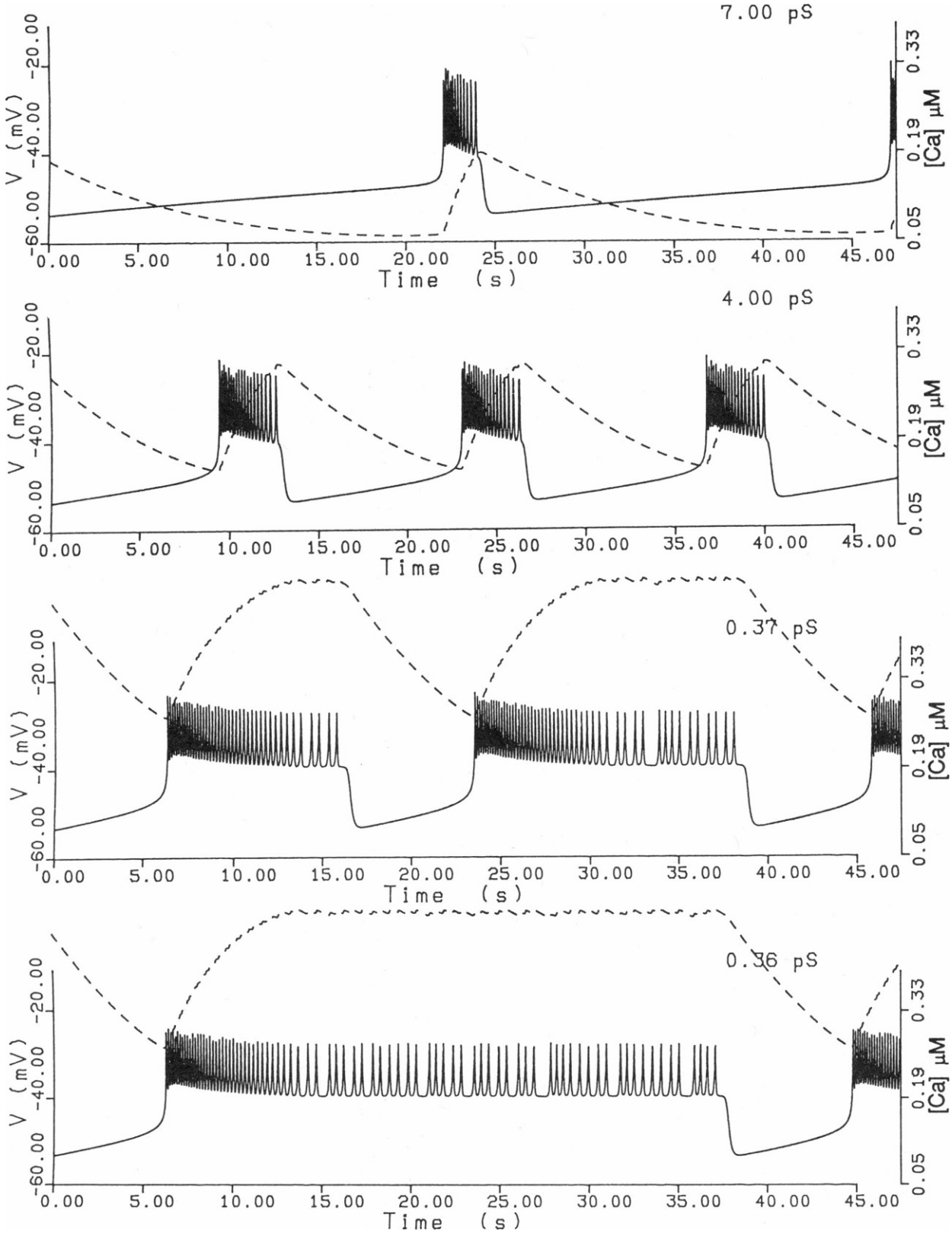

FIGURE 5 Potential vs. time for various values of $g_{K,ATP}$. For each trace, the value of $g_{K,ATP}$ is displayed in the upper-right-hand corner, and is expressed in picoSiemens (pS). Superimposed on the time course of membrane potential (mV, *solid line*) is the time course of intracellular calcium concentration (μM, *dashed line*). Time is in seconds.

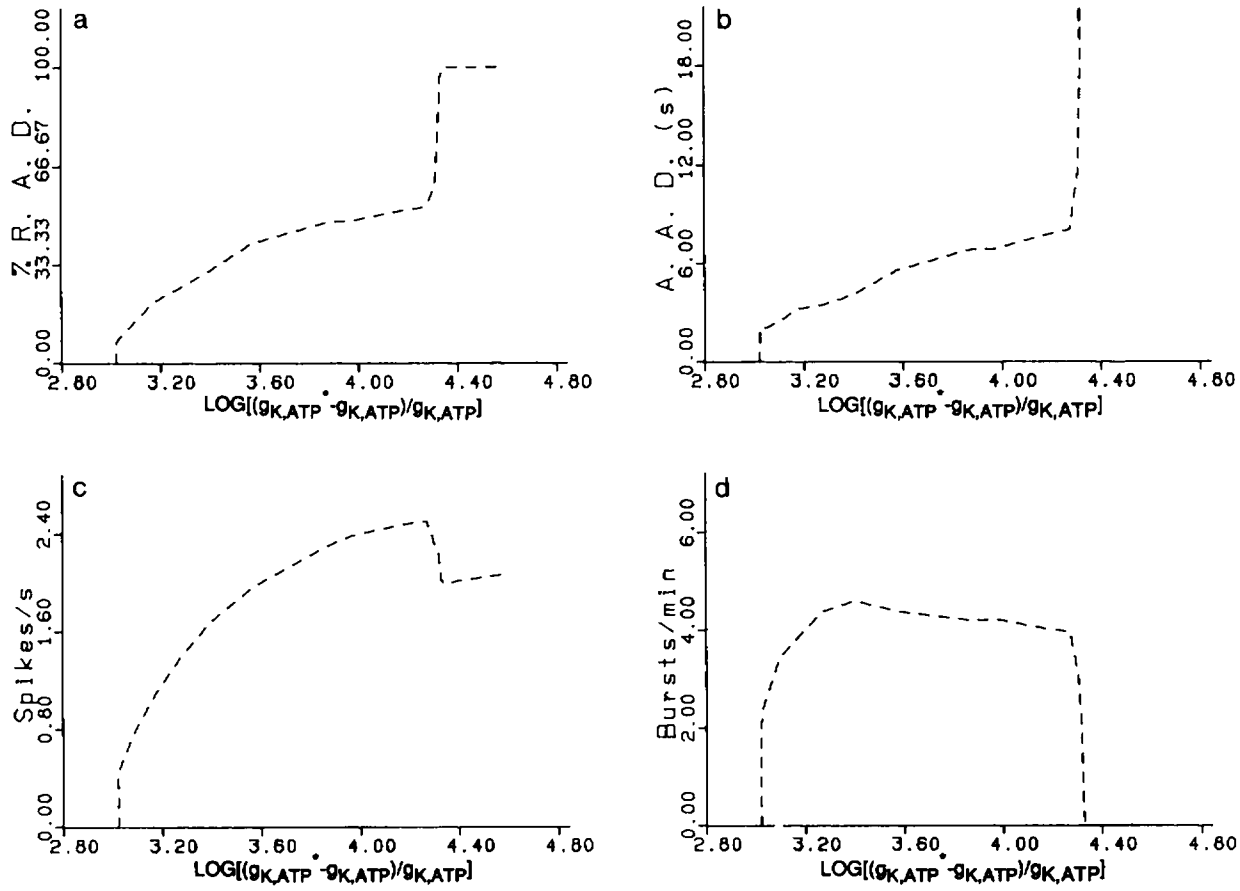

FIGURE 6 Effect of the ATP-inactivated K^+ channel on various dose response curves. The ordinate is log $[(g^*_{K,ATP} - g_{K,ATP})/g_{K,ATP}]$. Shown are (*a*) %RAD, (*b*) AAD (s), (*c*) spike frequency (s^{-1}), and (*d*) burst frequency (min^{-1}). $g^*_{K,ATP}$ was taken to be 7,500 pS.

values tested. The flux for $I_{K,V} + I_{K,Ca}$ gives a curve shaped much like that of $[Ca^{2+}]_i$. It ranges from 0.772 pmol/s per cm^2 at the onset of bursting to 3.83 pmol/s per cm^2 just before continuous spiking, and then jumps to and levels off at ~4.25 pmol/s per cm^2 during continuous spiking. Before the onset of electrical activity, the ATP-inactivated K^+ flux ($J_{K,ATP}$) dominates the total K^+ flux and gives it a concave-down tail which begins at 1.775 pmol/s per cm^2. $J_{K,ATP}$ continues along its concave-down trajectory until it reaches an inflection point shortly after the onset of electrical activity. From then on, it slowly approaches zero along a concave-up trajectory. Thus, the total flux, $J_{K,total}$, is dominated by the ATP-inactivated current for small x-axis values and by the Ca^{2+}-sensitive and the voltage-gated currents for large x-axis values.

Case III: pH Effect

In these simulations, the apparent dissociation constant, K_{dis}, of Ca^{2+} ions from the Ca^{2+}-activated voltage-gated K^+ channel was varied. k_{Ca} was held constant at 0.0450 ms^{-1}, a value for which continuous spiking occurred in the Case I simulations. $g_{K,ATP}$ was set equal to zero. It was assumed that protons competed competitively for the Ca^{2+} activation site on the Ca^{2+}-activated K^+ channel. Thus, K_{dis} could be associated with proton concentration by the following equation:

$$K_{dis} = K^*_{dis}\,(1 + [H^+]/K_a), \qquad (1)$$

where K^*_{dis} is defined as the actual dissociation constant in the absence of H^+ inhibition, and K_a is the K_i binding constant for H^+. H^+ is a function of glucose concentration. As glucose concentration increases, so does H^+ concentration. Thus, following reasoning similar to that used in Cases I and II, we assume that log $\{[\text{glucose}]/K_m\}$ is proportional to log $[(K_{dis} - K^*_{dis})/K^*_{dis}]$. Eq. 1 does not appear in the equations for our model, nor does K^*_{dis}. Thus, K^*_{dis} and K_a are not critical parameters in our model and have no direct bearing on the results.

Simulations were conducted for values of K_{dis} ranging from 0.027 μM to 25.00 μM. To use this entire range for the plots, K^*_{dis} was given the value of 0.020 μM. It is conceivable that only a very small region of the curves represented here are physiologically relevant. By choosing different values of K^*_{dis} and K_a, we can adjust the pH scale with respect to the x-axis. The choice will depend on the outcome of investigations into the time course of pH in

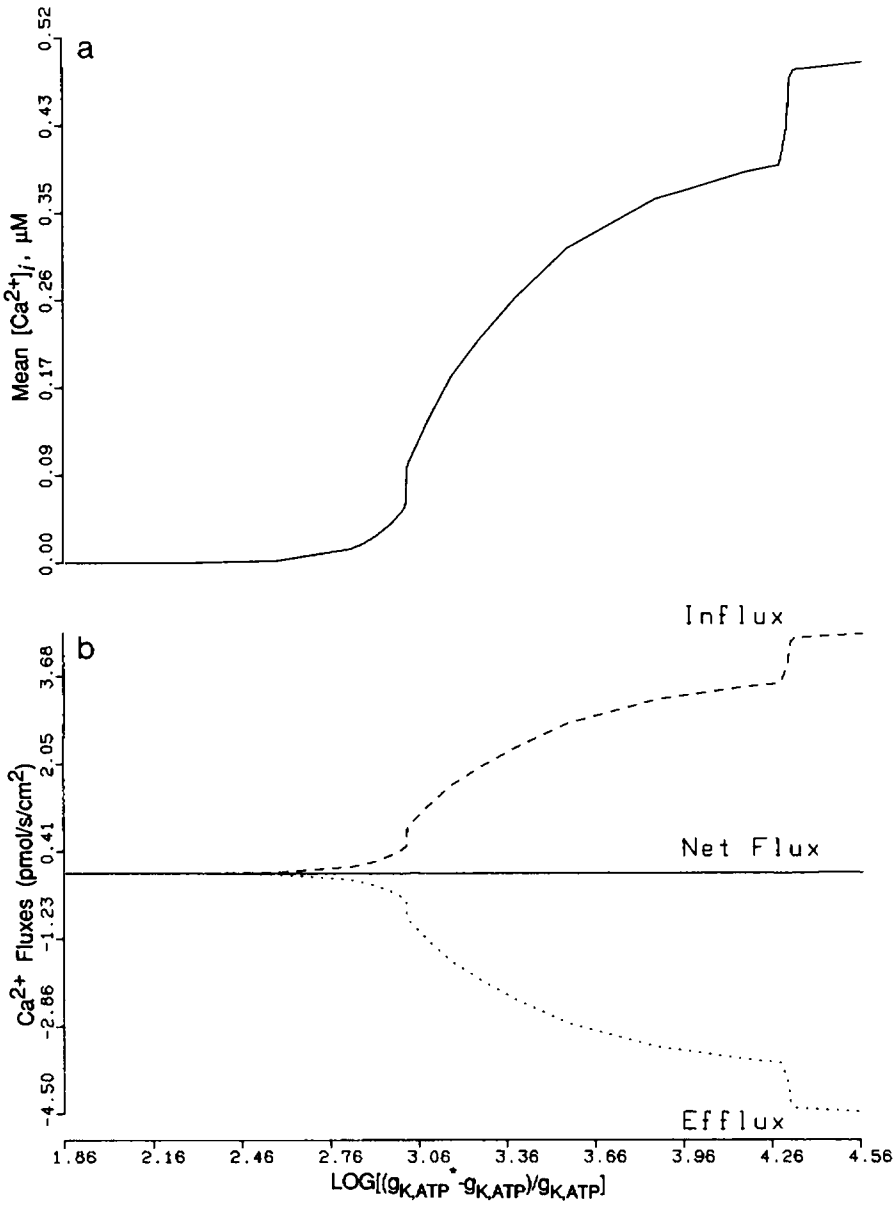

FIGURE 7 Effect of ATP-inactivated K^+ channel on (*a*) mean intracellular Ca^{2+} concentration (μM) and (*b*) Ca^{2+} fluxes (pmol/s per cm^2). The ordinate is log $[g^*_{K,ATP} - g_{K,ATP})/g_{K,ATP}]$. (*b*) *Dotted line*, efflux; *dashed line*, influx; *solid line*, net flux.

β-cells during glucose stimulation. Again, the choice of these parameters is not critical to the results presented here.

Fig. 9 shows plots of voltage and $[Ca^{2+}]_i$ with respect to time using a similar format as Fig. 5. K_{dis} is printed in the upper-right-hand corner of each plot and is expressed in micromolar. Once again, we see that the active phase gradually takes over and the silent phase becomes shorter and less frequent as K_{dis} increases (decreasing pH). The last plot demonstrates deterministic chaos at K_{dis} = 1.927 μM. By K_{dis} = 2.00 μM, continuous spiking occurs (not shown).

Fig. 10 illustrates some dose–response curves under Case III conditions. As before, the plots shown are %RAD, AAD, spike frequency, and burst frequency, all as a function of log $[(K_{dis} - K^*_{dis})/K^*_{dis}]$ in this instance. The curves all have the same basic shape as the corresponding curves from Cases I and II.

$[Ca^{2+}]_i$ behaves in a manner that on first inspection closely resembles that of Case II; that is, minimum $[Ca^{2+}]_i$, maximum $[Ca^{2+}]_i$, and the amplitude of the periodic fluctuation in $[Ca^{2+}]_i$ increase as K_{dis} decreases. However, Fig. 11 tells a somewhat different story. Here, $[Ca^{2+}]_i$ is plotted against log $[(K_{dis} - K^*_{dis})/K^*_{dis}]$. The curve is a smooth sigmoid, in sharp contrast to the equivalent curves for either of Case I or Case II.

The K^+ fluxes are shown in Fig. 12. The total K^+ flux, $J_{K,total}$, is also sigmoidal, ranging from ~0.9 pmol/s per cm^2

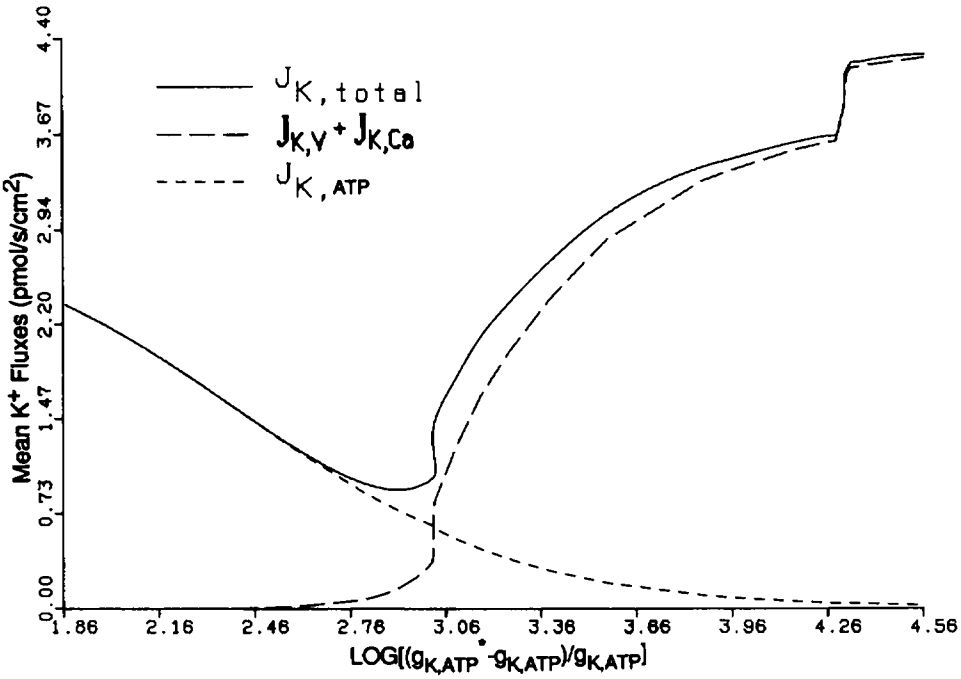

FIGURE 8 Effect of ATP-inactivated K^+ channel on K^+ efflux. The ordinate is log $[(g^*_{K,ATP} - g_{K,ATP})/g_{K,ATP}]$. Fluxes are in pmol/s per cm^2

for low x-axis values (resting potential) to 8.5 pmol/s per cm^2 at high x-axis values (continuous spiking).

DISCUSSION

The analysis presented here simulates three separate hypothetical effects of glucose on the β-cell. Results for Cases I and II ideally might be represented on a four-dimensional plot containing log $[k_{Ca}/(k^*_{Ca} - k_{Ca})]$ on the x-axis, log $[g^*_{K,ATP} - g^*_{K,ATP})/g_{K,ATP}]$ on the y-axis, log $[K_{dis} - K^*_{dis})/K^*_{dis}]$ on the z-axis, and the dependent variable on a fourth axis, K^+ flux, for instance. Our approach is simplified in each case by holding all parameters constant except one. For example, in Case I, $g_{K,ATP}$ and K_{dis} are fixed and k_{Ca} is varied. Moreover, the parameters k_{Ca}, $g_{K,ATP}$, and K_{dis} are treated as independent variables since we do not know their precise mathematical relationship to glucose concentration. In Case I, so long as we choose values of $g_{K,ATP}$ and K_{dis} for which spikes will occur, the exact values chosen are not critical; indeed, the same qualitative results are obtained whether $g_{K,ATP}$ is set equal to zero or equal to 5 pS. Likewise, in Case II, we hold both k_{Ca} and K_{dis} constant, and in Case III we hold k_{Ca} and $g_{K,ATP}$ constant. Thus, each case explores the dependence of the model on only a single parameter, while all other parameters are fixed.

In the following discussion, the independent variable, a hypothetical function of glucose concentration, will be referred to as $X(G)$ in all three cases. Also, when we say "pre-bursting $X(G)$ interval," we are referring to low values of $X(G)$ for which no bursts occur and the membrane voltage remains at resting potential in the simulation. This is analogous to the resting cell state, during which glucose concentration is low. We will discuss how our results compare with experimental results, illustrating how the methods reported here can help evaluate a mathematical model for the β-cell. Then, we will discuss the role of the ATP-inactivated K^+ channel and the Ca^{2+}-activated K^+ channel as related to our model.

Each of the three cases predicted different shaped curves for $[Ca^{2+}]_i$ versus glucose concentration (compare Figs. 3, 7, and 11). For Cases II and III, we calculated a net increase in $[Ca^{2+}]_i$. By contrast, Case I gave a net decrease $[Ca^{2+}]_i$ until the onset of continuous spiking. In large part, that decrease resulted from the relatively high $[Ca^{2+}]_i$ tail calculated for the pre-bursting $X(G)$ interval. Insulin secretion, which occurs only during active electrical activity, should be accompanied by a net increase in $[Ca^{2+}]_i$. The high $[Ca^{2+}]_i$ tail for the pre-bursting domain in Case I is thus not supported by experimental findings. That this problem does not occur in Case II, which contains the ATP-inactivated K^+ channel, may show the importance of $I_{K,ATP}$ in the pre-bursting domain (i.e., in the resting cell). It should be possible to test these computed predictions using Quin2 experiments such as were performed by Rorsman et al. (34). However, care must be taken to distinguish between phase 1 (transient) and phase 2 (the limit cycle, or steady-state phase) of the biphasic response.

The curves for mean spike frequency versus glucose concentration, produced by each of the three cases, closely resemble the experimental results of Scott et al. (36). The typical curve was concave-down, started at zero spikes per second at the threshold glucose concentration, increased up

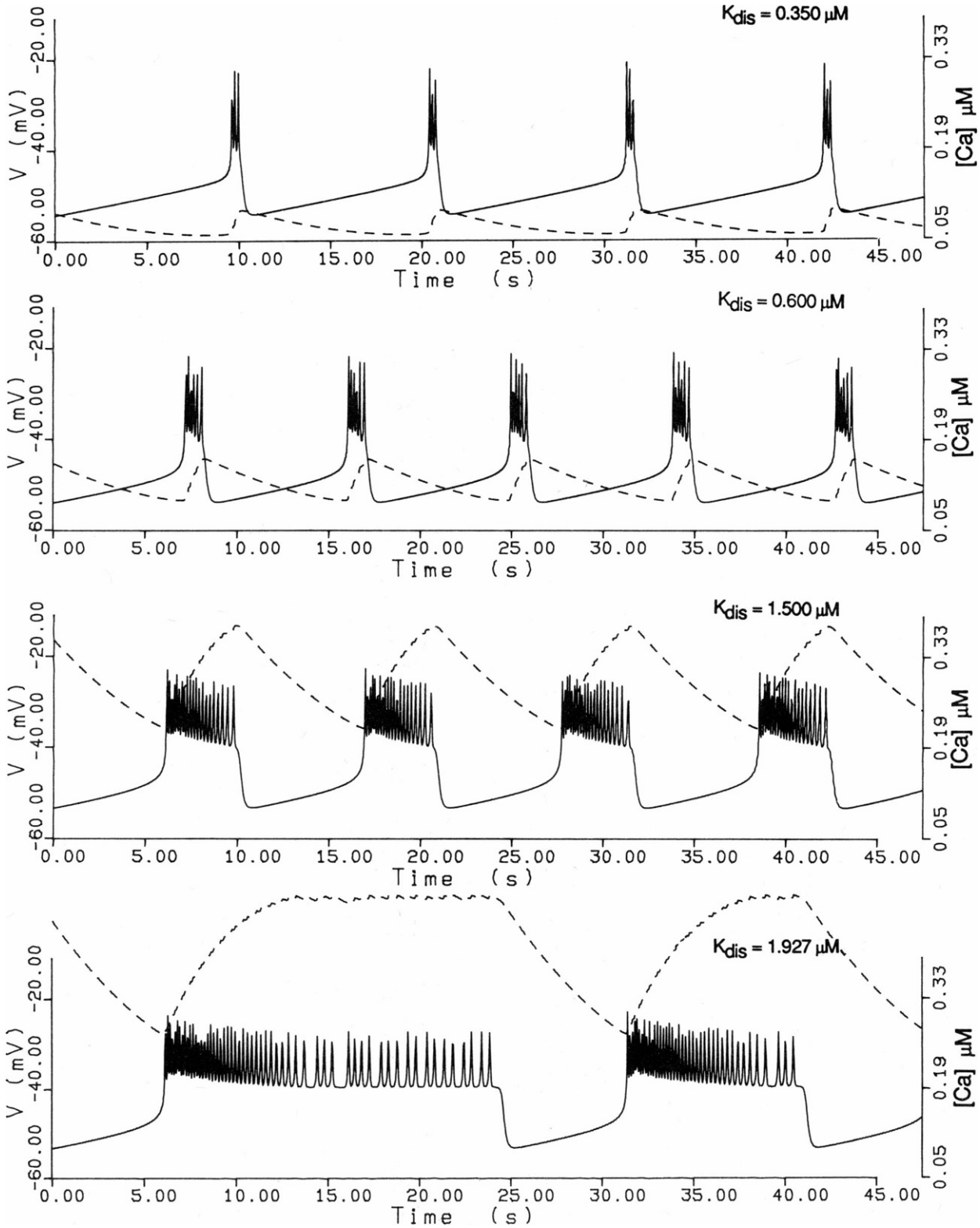

FIGURE 9 Potential vs. time for various values of K_{dis}. For each trace, the value of K_{dis} is displayed in the upper-right-hand corner, and is expressed in micromolar (μM). Superimposed on the time course of membrane potential (mV, *solid line*) is the time course of intracellular calcium concentration (μM, *dashed line*).

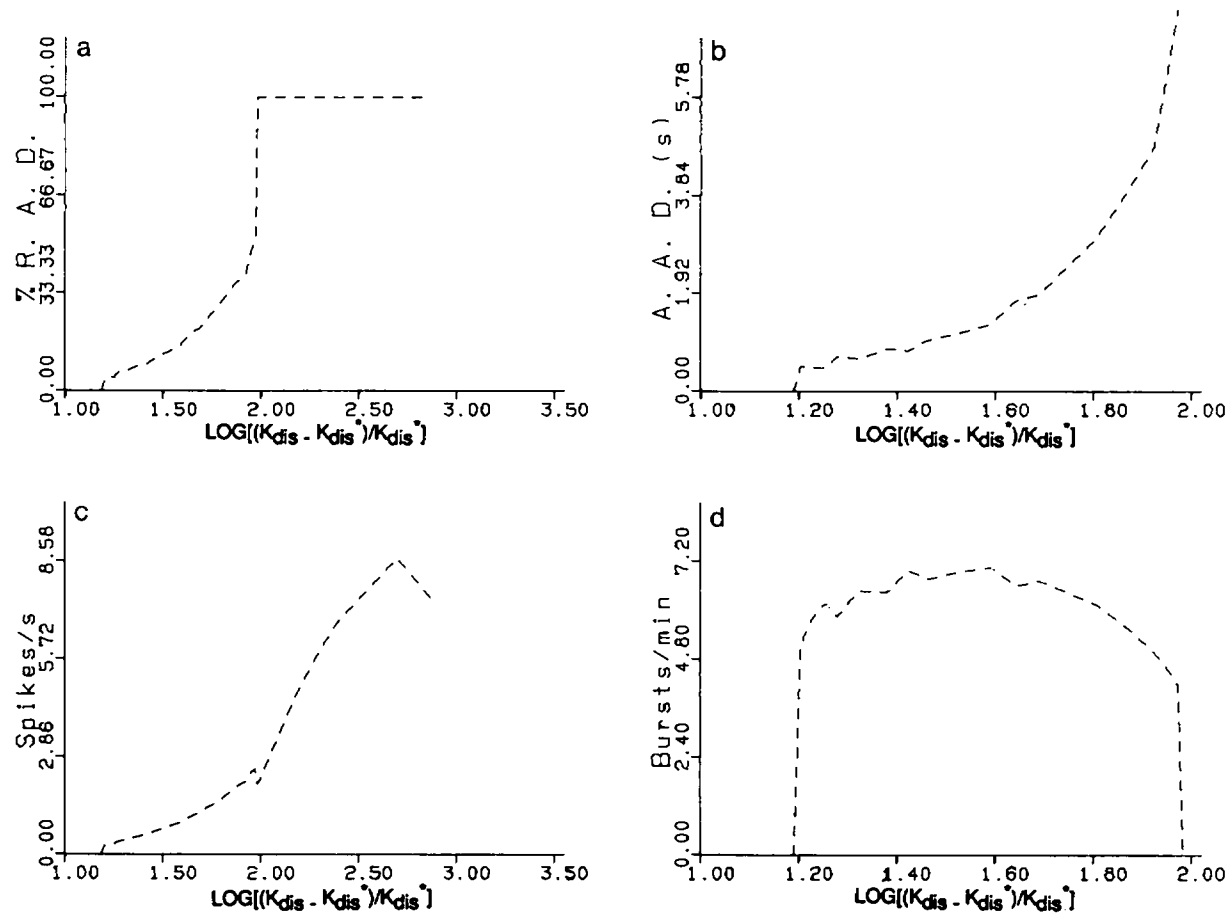

FIGURE 10 Effect of pH on various dose response curves. The ordinate is log $[(K_{dis} - K^*_{dis})/K^*_{dis}]$ Shown are (*a*) %RAD, (*b*) AAD (s), and (*c*) spike frequency (s^{-1}), and (*d*) burst frequency (min^{-1}). K^*_{dis} was taken to be 0.02 μM.

to the point where continuous spiking occurred, and then decreased slightly (compare Figs. 2, 6, and 10).

The curves presented here for %RAD versus glucose concentration differ in their detail from the curve obtained experimentally by Meissner and Preissler (29). The curve they reported is sigmoidal, gradually rising from 0% to an inflexion point near 50% and levelling off at 100%. The curves presented here differ in two ways. First, the ones from Cases I and II rise abruptly from 0% in a concave-down fashion. Secondly, the curves of all three cases lack a well defined inflexion point, and they jump brusquely from near 50% to 100% in the neighborhood of onset of continuous spiking.

Three explanations may be offered for the apparent discrepancies. First, and most significantly, Meissner and Preissler included both phases of the biphasic response in their calculation of %RAD (referred to by them as "% time at plateau level") (29), whereas our Case I and II simulations are concerned only with the limit cycle. In Case III here, we see that the pH effect leads to a gradual, concave-up increase in %RAD from zero. As will be discussed later, it is possible that the pH effect plays a prominent role in the first phase of the biphasic response. An averaging of the Case III curve with the %RAD curve from either of the other two cases ought to produce a result closer to that reported experimentally. Second, the data points that Meissner and Preissler used were means of several different cells, presumably from different islets. But electrical response to glucose (such as in the precise duration of limit cycle bursts for a given glucose concentration) varies from islet to islet in the same preparation (4). If all the data points had reflected burst duration of a single cell, it is possible that the curve Meissner and Preissler obtained might have more closely resembled the curve for %RAD that we obtained for simulations of a single cell. Finally, the Meissner and Preissler plot contains relatively few data points, allowing some leeway in interpreting the exact shape of the curve.

Total K^+ efflux as a function of $X(G)$ showed a somewhat sigmoidal relationship for all three cases. However, there were differences. Most significantly, at low $X(G)$ below the threshold for burst activity, Case II ($I_{K,ATP}$ present) gave a negative slope tail that began at ~1.8 pmol/s per cm^2 and dropped down to ~0.9 pmol/s per cm^2 before the curve began to increase again (see Fig. 8). No such decrease was seen in the curves for either Case I or Case III, although a slight decrease was seen in Case I from ~1.0 to 0.9 pmol/s per cm^2 (see Figs. 4 and 12).

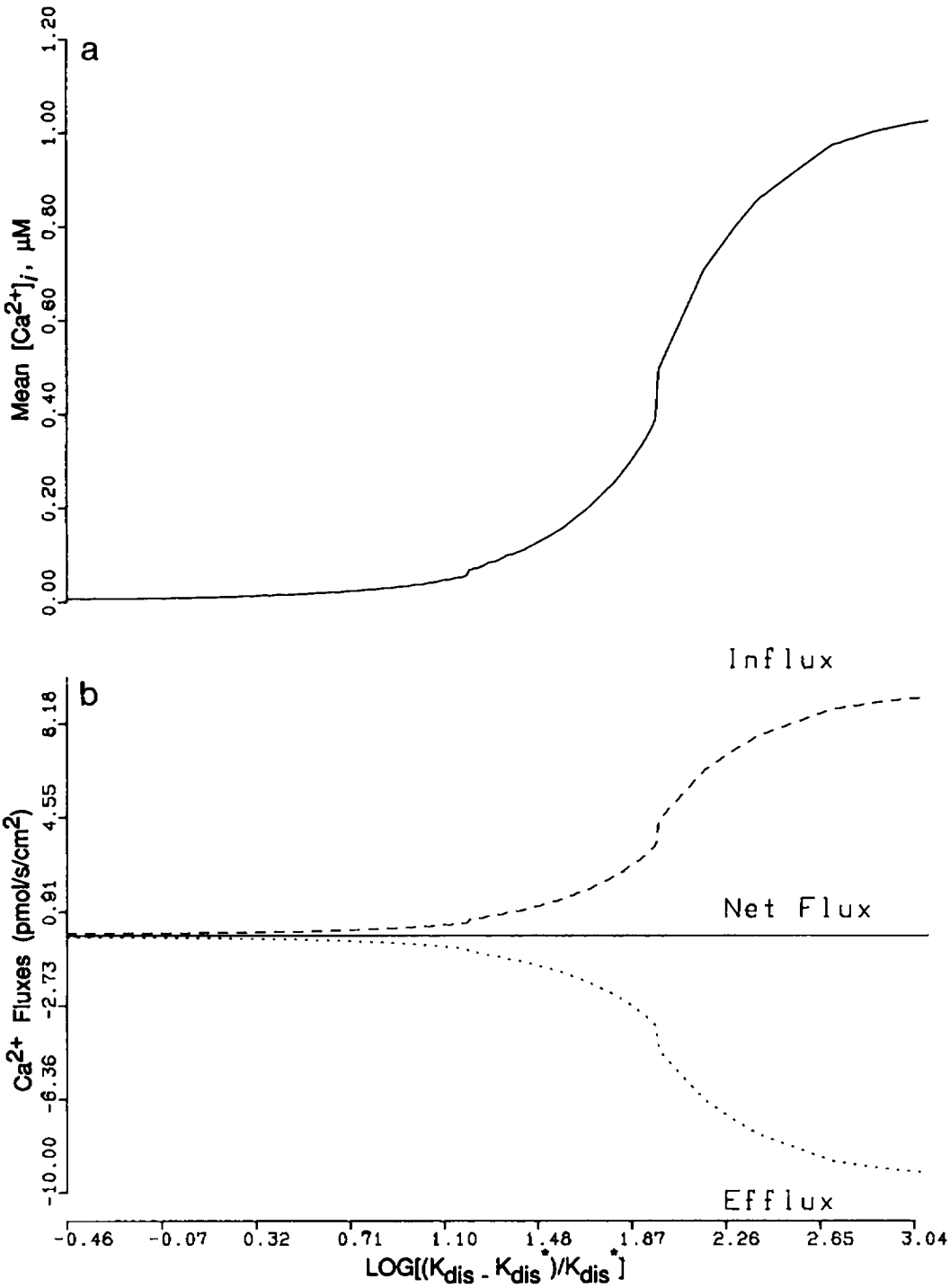

FIGURE 11 Effect of pH on (*a*) mean intracellular Ca^{2+} concentration (μM) and (*b*) Ca^{2+} fluxes (pmol/s per cm^2). The ordinate is log $[(K_{dis} - K_{dis}^*)/K_{dis}^*]$. (*b*) *Dotted line*, efflux; *dashed line*, influx; *solid line*, net flux.

Henquin (20, 22) using $^{42}K^+$ and $^{86}Rb^+$ as tracers, studied K^+ efflux from perfused rat pancreatic islets as a function of glucose concentration. Instead of getting the roughly sigmoidal relationship computed here, he got a curve that closely resembles the curve for the $I_{K,ATP}$ efflux simulated here. That our results for Case II predict greater total K^+ flux during large $X(G)$ (continuous spiking) than small $X(G)$ (no spiking) may reflect an inadequacy of our equation for I_g at low (negative) membrane potentials (more later). Nevertheless, it is worth pointing out that Case II alone produced a concave-down tail for the pre-bursting $X(G)$ interval (compare Figs. 4, 8, and 12), so that, out of the three cases, Case II most closely approached the experimental K^+ flux curve. This may

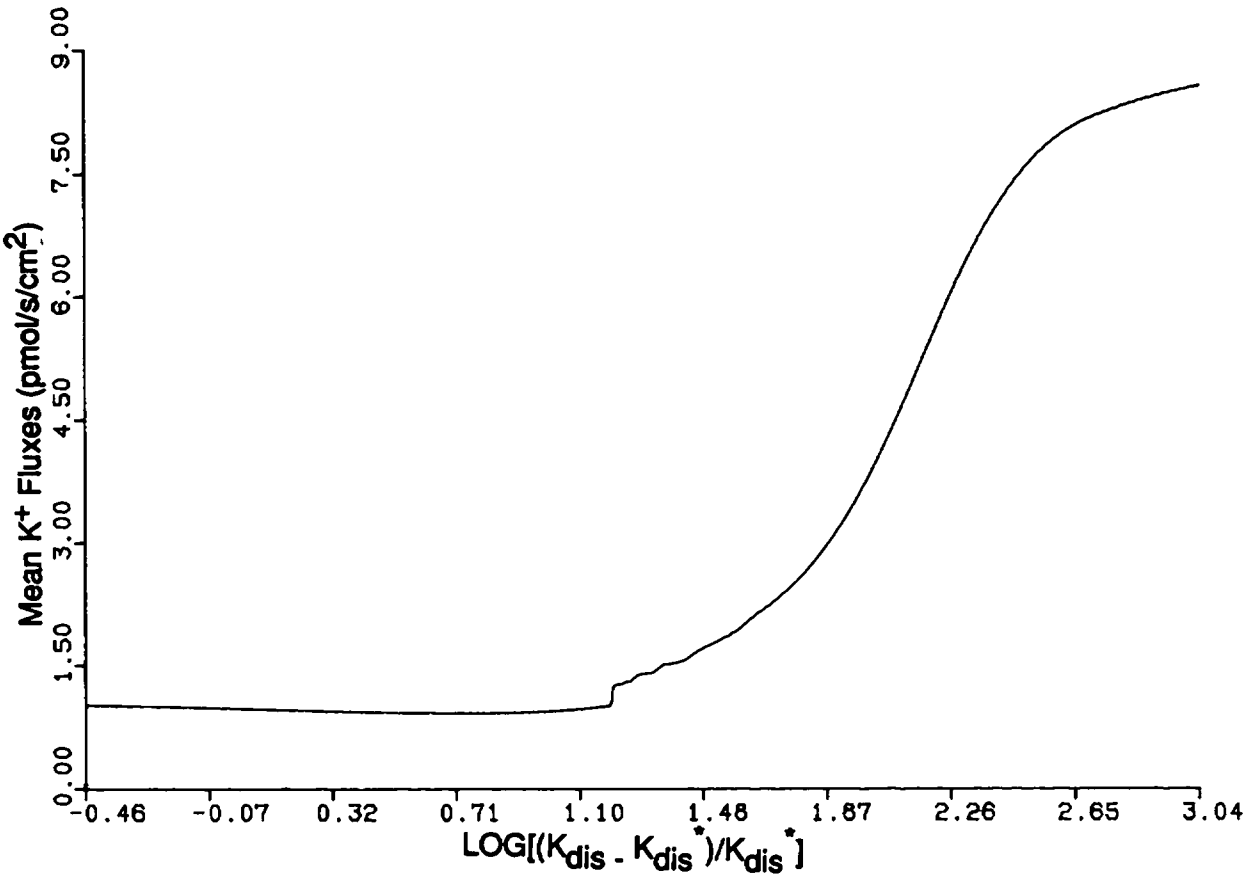

FIGURE 12 Effect of pH on K^+ efflux. The ordinate is log $[(K_{dis} - K^*_{dis})/K^*_{dis}]$. Fluxes are in pmol/s per cm^2.

indicate that $I_{K,ATP}$ is an important component of the total K^+ flux for the pre-bursting domain.

We noted in Case II that for large $g_{K,ATP}$ (>~100 pS) the resting membrane was hyperpolarized to −80 mV or lower. Under these conditions, the only ionic currents of significance were $I_{K,ATP}$ and the leak current. We found that the leak current was not great enough to maintain the resting potential at −70 mV. Thus, our leak current may be too simple and not applicable all the way down to −70 mV. Satin and Cook (35) reported β-cell leak conductances ranging from 83 pS to 1,000 pS during voltage clamps to potentials negative of a −50 mV holding potential. When we used a leak current conductance of 100 pS and large $g_{K,ATP}$ (>1,000 pS), a large net K^+ flux was observed of the sort that should corroborate the Henquin $^{42}K^+$ tracer experiments mentioned earlier. We suggest that components of the leak current may require inward rectification and/or some glucose dependence to maintain the experimentally observed resting potential in low glucose.

Adjusting the leak conductance to 100 pS in Cases I and III cannot produce a K^+ efflux curve like Henquin's unless $[Ca^{2+}]_i$ is very high for pre-bursting $X(G)$ intervals, because K^+ flux is completely due to $I_{K,V} + I_{K,Ca}$ in Cases I and III.

The Case III simulations may provide some insight into the basis of the biphasic response of β-cells to glucose elevation. As previously mentioned, experiments by Rorsman et al. (34) and by Herchuelz and Malaisse (24) show that sequestration of intracellular Ca^{2+} is active during the transient phase. Studies in other systems indicate that mitochondria take up Ca^{2+} via an H^+–Ca^{2+} exchange (28). This raises the possibility that the observed sequestration of intracellular Ca^{2+} in β-cells may be due to an uptake of Ca^{2+} by the mitochondria, and that this uptake of Ca^{2+} is accompanied by a release of protons. As previously indicated, Cook et al. (15) reported that low pH inhibits the Ca^{2+}-activated K^+ channel in the β-cells of neonatal rats. If enough protons are released during the proposed H^+–Ca^{2+} exchange to overcome the buffering power of the cytosol, then the initial drop in $[Ca^{2+}]_i$ in response to glucose stimulation reported by Rorsman et al. (34) and by Herchuelz and Malaisse (24) might be accompanied by a transient drop in cytoplasmic pH, which, in turn, could lead to inhibition of the $I_{K,Ca}$ current. It has yet to be established that the mitochondria acidify the cytosol temporarily in response to glucose.

Nevertheless, it might be hypothesized that, upon elevation of glucose to threshold levels, the mitochondria acidify the cytosol during oxidative phosphorylation and Ca^{2+}

uptake, that the cell gradually restores the cytosolic pH to resting levels via Na^+–H^+ exchangers in the plasma membrane, and that the transient drop in pH inhibits the Ca^{2+}-activated K^+ channels temporarily. This transient inhibition would lead to the long first phase of electrical activity, and, as pH returned to normal, the Ca^{2+}-activated K^+ channels would be reactivated, resulting in repolarization. Further modulation of these channels would be controlled chiefly by fluctuations in $[Ca^{2+}]_i$ during the second phase of electrical activity. Thus, it is proposed that the biphasic electrical activity seen in β-cells results from the temporary inactivation of the Ca^{2+}-activated K^+ channels during a transient initial drop in cytosolic pH produced during Ca^{2+}–H^+ exchange at the mitochondria (9).

Experiments to elucidate the cytoplasmic pH time course during glucose stimulation indicate that pH rises after several minutes in high glucose perfusion media (27). However, the design of these experiments prevents determination of pH during the first 7 min after introduction of the high glucose media. Consequently, these experiments do not measure pH during the first phase of the biphasic response and therefore do not contradict our hypothesis. Pace (31) showed that when the cytosolic pH was decreased in the presence of subthreshold glucose levels, electrical activity could be induced. In suprathreshold glucose levels, continuous spiking or a biphasic response could be induced when the intracellular pH was lowered by various techniques.

Atwater et al. (3, 4) suggested that glucose may metabolically lower the affinity for Ca^{2+} at the proposed Ca^{2+}-activated K^+ channel, and that this along with $[Ca^{2+}]_i$ might enable that channel to control both the resting potential and bursting phenomenon in β-cells. If this interpretation were entirely correct, then the role of ATP-inactivated K^+ channel would also be served by the Ca^{2+}-activated K^+ channel. Indeed, one could argue that the Atwater hypothesis is supported by the findings of Rorsman et al. (34) and of Herchuelz and Malaisse (24) that glucose stimulation may lead initially to a transient drop in $[Ca^{2+}]_i$ before the onset of Ca^{2+} influx through voltage-gated channels. In low glucose concentrations, the Ca^{2+}-activated K^+ channel could be activated by relatively low concentrations of intracellular free calcium. Then, two things could happen. First, a brief initial drop in $[Ca^{2+}]_i$ due to sequestration could shut down this channel. Then, a rise in some glucose metabolite could lower the channel's affinity for Ca^{2+}, so that a much higher concentration is needed to reactivate it sufficiently to repolarize the plasma membrane. Under these latter conditions, the channel would trigger the silent phases between bursts. However, evidence that a distinct and separate ATP-inactivated K^+ channel coexists with the Ca^{2+}-activated voltage-gated K^+ channel supplies us with a simpler alternative model, in which the ATP-inactivated K^+ channel determines the resting potential and the Ca^{2+}-activated K^+ channel dominates the silent phase.

Cook and Hales (14) reported that 100 μM quinine inhibits the ATP-inhibited K^+ channel. Findlay et. al. (19) corroborated this finding and also reported that 2 mM tetraethylammonium (TEA) selectively inhibits the Ca^{2+}-activated voltage-gated K^+ channel. Studies by Henquin with TEA (22) and by Atwater et al. (5) with TEA and quinine thus lend themselves easily to interpretations involving the ATP-inactivated K^+ channel. Henquin reported that, in the presence of 6 mM glucose, 20 mM TEA reduced $^{86}Rb^+$ efflux, depolarized β-cell membranes, led to insulin release, and prevented repolarization. However, in 0 or 3 mM glucose, TEA could not reduce $^{86}Rb^+$ efflux enough to depolarize the cells to the threshold for electrical activity, and no insulin release occurred. This suggests that TEA alone cannot inactivate the potassium channel which dominates the resting potential.

Although Atwater et al. (5) said that resting potential was unaffected by TEA, they indicated that TEA reduced the threshold glucose concentration necessary to elicit electrical activity, and they found, much like Henquin, that TEA could not elicit electrical activity in the absence of glucose. Quinine (100 μM), which they regarded as a blocker of the Ca^{2+}-activated K^+ channel, could induce electrical activity in the absence of glucose (3). An alternative interpretation to the one favored by the Atwater group is that quinine inhibits the ATP-inactivated K^+ channel, leading to electrical activity. This is consistent with the clamp patch experiments of Findlay et al. (19).

The Atwater group introduced mitochondrial uncouplers and inhibitors into the medium of perfused mouse β-cells to liberate calcium from the mitochondria and activate the Ca^{2+}-sensitive K^+ channel (3). The uncouplers 2,4-dinitrophenol (DNP), *m*-chlorophenylhydrazone (CCCP), *p*-trifluoromethoxyphenylhydrazone (FCCP), and the inhibitors potassium cyanide (KCN) and sodium azide (NaN_3) were tried. In 11.1 mM glucose Krebs, each of these induced hyperpolarization (and zero electrical activity). The effect was reversible, and removal of the inhibitor or uncoupler led to bursts of electrical activity following a biphasic pattern much like what is seen when glucose is added to a glucose-deprived medium. When quinine was added to the perfusate, it partially or completely inhibited the effect of the mitochondrial inhibitors and uncouplers. The explanation they offered for this behavior was that the release of Ca^{2+} from the mitochondria, induced by the uncoupler or inhibitor, elevated $[Ca^{2+}]_i$ and thereby activated the Ca^{2+}-activated K^+ channel sufficiently to polarize the plasma membrane below threshold levels. Quinine inhibited this effect by blocking this K^+ channel (3).

Cook and Hales (14) offered an alternative explanation. They contended that the drop in intracellular ATP caused by the mitochondrial uncouplers or inhibitors led to activation of the ATP-inactivated K^+ channel, which, in turn, polarized the cell (as previously mentioned, they also reported that quinine causes inhibition of the ATP-

inactivated K^+ channel [14]). It is likely that both the Atwater et al. and the Cook–Hales mechanisms were at work. However, consistent with the view of this paper that the ATP-inactivated K^+ channel dominates the resting potential while the Ca^{2+}-activated K^+ channel dominates the silent phase between bursts, the Cook–Hales mechanism is probably most significant.

In summary, the simulations reported here predict curves for $[Ca^{2+}]_i$ and K^+ fluxes as an indirect function of glucose concentration for three separate hypotheses that attempt to explain the glucose regulation of electrical activity. The first hypothesis, first put forward by the Atwater group, proposes that Ca^{2+}-activated K^+ channels are responsible for both resting potential and the silent phase during limit cycle bursting, and that the glucose dependency of the bursting activity is attributable to glucose modulation of the Ca^{2+} sequestration and efflux processes. The second hypothesis holds that the ATP-inactivated K^+ channels dominate the resting potential, while the Ca^{2+}-activated K^+ channels are the main contributor to the silent phase during bursting. The third hypothesis, which is probably most relevant for the first phase of the characteristic biphasic response, holds that the Ca^{2+}-activated K^+ channels are inhibited during a transient drop in pH, leading to an abnormally long burst of spike activity. Although the present model presents the Ca_i-sensitive and voltage-gated component as the sum of two distinct currents, $I_{K,Ca}$ and $I_{K,V}$, preliminary indications are that qualitatively similar results are obtained when these two currents are combined into one current whose conductance is both Ca^{2+}-activated and voltage-gated (11). Our model therefore makes reasonable allowance for presently available experimental evidence. The plots of $[Ca^{2+}]_i$ and K^+ fluxes can be investigated experimentally to determine to what extent each of these hypotheses may contribute to the actual prevailing mechanisms for regulation of electrical activity and insulin release. The second two hypotheses appear to be favored by available experimental evidence. As more information becomes available on the properties of the ATP-inactivated K^+ channel and the leak current, this sort of numerical analysis can be conducted again to help evaluate the viability of particular hypotheses on the electrophysiology of pancreatic β-cells.

APPENDIX A

Explanation of Equations Used in the Model

$[Ca^{2+}]_i$ is a dynamic variable given by Eq. A1.

$$f^{-1}\frac{d[Ca^{2+}]_i}{dt} = \frac{3I_{Ca,v}}{4\pi r^3 F} - k_{Ca}[Ca^{2+}]_i. \quad \text{(A1)}$$

In Eq. A1, k_{Ca} is a rate constant to account for Ca^{2+} efflux and sequestration from the cytosol by various energy-requiring sequestration processes. A simple rate expression (i.e., $k_{Ca}[Ca^{2+}]_i$) is used for the efflux term in place of a Michaelis–Menton equation or Hill equation because simulations using these equations yield essentially the same results (11), as reported here. Moreover, since use of the Michaelis–Menton or Hill equation makes use of additional parameters (i.e., the Hill coefficient and the binding constant), we find no advantage to using either one. In Eq. A1, f is related to the fraction of free Ca^{2+} ions, and $I_{Ca,v}$ is the current through the voltage-gated Ca^{2+} channel and is given by Eq. A2:

$$I_{Ca,V} = \bar{g}_{Ca} m_\infty^3 h_\infty (V_{Ca} - V). \quad \text{(A2)}$$

Here, V_{Ca} is the reversal potential for Ca^{2+}, $\bar{g}_{Ca}$ is the maximum conductance, and m_∞ and h_∞ are the steady-state Hodgkin–Huxley activation and inactivation variables. m_∞ and h_∞ are described by Eq. A3, where y is either m_∞ or h_∞.

$$y_\infty = \frac{\alpha_y}{\alpha_y + \beta_y}. \quad \text{(A3)}$$

The equations for the respective voltage-sensitive kinetics constants, α_y and β_y, have the same forms as the original Hodgkin–Huxley equations (26), but the voltage axis has been shifted by 50 mV. These kinetics equations are given in Table AI.

The current, $I_{K,ATP}$, through the ATP-inactivated K^+ channel, is described by Eq. A4:

$$I_{K,ATP} = g_{K,ATP}(V_K - V), \quad \text{(A4)}$$

where $g_{K,ATP}$ is the conductance through the ATP-inactivated K^+ channel. It is assumed that $g_{K,ATP}$ decreases as glucose concentration increases. Since the precise mathematical and mechanistic relationship between glucose concentration and $g_{K,ATP}$ is not presently known (1) we have taken the ATP-inactivated K^+ channel conductance to be time independent.

There are two other potassium currents: A Ca^{2+}-dependent current ($I_{K,Ca}$) and a voltage-dependent current ($I_{K,V}$). The voltage-gated component is given by Eq. A5. It has the same general form as the Hodgkin–Huxley equation (26):

$$I_{K,V} = \bar{g}_{K,V} n^\ell (V_K - V), \quad \text{(A5)}$$

where V_K is the reversal potential for K^+, and V is the membrane potential. $\bar{g}_{K,V}$ is the conductance through the channel when it is fully activated, and n is the probability of opening the channel. The exponent, ℓ, is a positive integer chosen empirically for the best fit with experimental data, when available. In the absence of experimental data, we arbitrarily chose a value of 3 for ℓ. The variable, n, has kinetics that are defined by Eq. A6:

$$\frac{dn}{dt} = \frac{\lambda[n_\infty - n]}{\tau_n}, \quad \text{(A6)}$$

where λ is a proportionality constant, n_∞ is n at the steady state, and τ_n is a relaxation time constant. The voltage dependencies of n_∞ and τ_n are based on the original Hodkin–Huxley equations (26). Thus, n_∞ is described by Eq. A7, and τ_n is described by Eq. A8:

$$n_\infty = \alpha_n \tau_n \quad \text{(A7)}$$

$$\tau_n = \frac{1}{\alpha_n + \beta_n}. \quad \text{(A8)}$$

TABLE AI
RATE EQUATIONS FOR VOLTAGE-GATED CALCIUM CURRENT

$\alpha_m = 0.1(-V - 25)/\{\exp[(-V - 25)/10] - 1\}$

$\beta_m = 4.0 \exp[(-V - 50)/18]$

$\alpha_h = 0.07 \exp[(-V - 50)/20]$

$\beta_h = 1/\{\exp[(-V - 20)/10] + 1\}$

TABLE AII
RATE EQUATIONS FOR VOLTAGE-GATED POTASSIUM CURRENT

$$\alpha_n = 0.01\,(-V - 20)/\{\exp[(-V - 20)/10] - 1\}$$

$$\beta_n = 0.125 \exp[(-V - 30)/80]$$

The constants, α_n and β_n, are voltage-sensitive rate constants for, respectively, the opening and closing of the "n" Hodgkin–Huxley gate in the voltage-gated K^+ channel. They have the same forms as the original Hodgkin–Huxley equations (26), but the voltage axis has been shifted by 30 mV. The equations for these rate constants are given in Table AII.

The Ca^{2+}-activated component, $I_{K,Ca}$, is described by Eq. A9:

$$I_{K,Ca} = \bar{g}_{K,Ca} \frac{[Ca^{2+}]_i/K_{dis}}{1 + [Ca^{2+}]_i/K_{dis}} (V_K - V). \qquad (A9)$$

Here, $[Ca^{2+}]_i$ is the intracellular calcium concentration, K_{dis} is the apparent dissociation constant of Ca^{2+} ions from the Ca^{2+}-activated voltage-gated K^+ channel, and $\bar{g}_{K,Ca}$ is the maximum conductance through this channel during Ca^{2+} saturation.

A more accurate mathematical model would combine $I_{K,Ca}$ and $I_{K,V}$ into one current whose conductance is a function of both $[Ca^{2+}]_i$ and membrane potential, in agreement with experimental evidence that a large-conductance voltage-gated K^+ current is also Ca^{2+}-activated (15, 17, 18). Such a model would be expected to produce results similar to our own for the total K^+ efflux. This is because the total flux is the sum of the fluxes for $I_{K,V}$ and $I_{K,Ca}$, and $I_{K,Ca}$ is small compared with $I_{K,V}$ in our computations. Our large-conductance voltage-gated K^+ current behaves like the β-cell voltage-gated Ca^{2+}-activated K^+ current would during relatively positive potentials. When we modified our model equations (10) by replacing $I_{K,Ca}$ and $I_{K,V}$ with one current whose conductance was both Ca^{2+}-activated and voltage-gated (more in agreement with experimental evidence), the mean $[Ca^{2+}]_i$ and mean K^+ flux analysis described here yielded qualitatively the same results (not shown) for Case I; namely, a net decrease in $[Ca^{2+}]_i$ occurred with respect to increasing $X(G)$, and the total K^+ flux curve did not have a concave-down tail for the pre-bursting domain. Preliminary simulations of Case II using the modified model just mentioned also yielded a similarly shaped curve as in Fig. 8.

The leak current, I_ℓ, is included to account for leakage of Na^+ and other ions across the plasma membrane (11). It is given by Eq. A10, where g_ℓ is the leak conductance and V_ℓ is the apparent reversal potential of leaking ions:

$$I_\ell = g_\ell(V_\ell - V). \qquad (A10)$$

Finally, the time derivative of the membrane potential V, is given by Eq. A11, where C_m is the membrane capacitance:

$$4\pi r^2 C_m \frac{dV}{dt} = I_{Ca,v} + I_{K,v} + I_{K,Ca} + I_{K,ATP} + I_\ell. \qquad (A11)$$

In the above equations, the reversal potentials for Ca^{2+} and K^+ are given, respectively, by Eqs. A12 and A13, where $[Ca^{2+}]_o$ is external Ca^{2+} concentration, $[K^+]_o$ is external K^+ concentration, $[K^+]_i$ is intracellular K^+ concentration, R is the gas constant, T is absolute temperature, and F is the Faraday constant:

$$V_{Ca} = \frac{RT}{2F} \ln \frac{[Ca^{2+}]_o}{[Ca^{2+}]_i} = 13.4 \ln \frac{[Ca^{2+}]_o}{[Ca^{2+}]_i} \qquad (A12)$$

$$V_K = \frac{RT}{F} \ln \frac{[K^+]_o}{[K^+]_i} = 26.7 \ln \frac{[K^+]^o}{[K^+]_i}. \qquad (A13)$$

APPENDIX B

Constants for β-Cell Equations

$\bar{g}_{Ca} = 7.0$ nS
$\bar{g}_{K,v} = 2.0$ nS
$\bar{g}_{K,Ca} = 60$ pS
$g_{K,ATP} = 0.0$ (or variable in Case II)
$g_\ell = 28$ pS
$V_\ell = 40$ mV
$[Ca^{2+}]_o = 2.0$ mM
$[K^+]_o = 5.0$ mM
$[K^+]_i = 130.0$ mM
$f = 0.002$
$K_{dis} = 2.0$ μM (or variable in Case III)
$k_{Ca} = 0.045$ ms^{-1} (or variable in Case I)
$r = 6.0$ μm
$\lambda = 1/0.003$
$C_m = 1$ μF/cm^2
$T = 310$ K
$F = 96487$ C/mol
$R = 8.314$ J/mol per K
$\ell = 3$

The choice of our parameters was discussed in Chay and Keizer (12).

We would like to express our gratitude to Dr. Illani Atwater at the National Institute of Health for her helpful discussions and suggestions during the course of this work.

This work was supported by grant PCM82-15583 from the National Science Foundation.

Received for publication 7 January 1986 and in final form 22 May 1986.

REFERENCES

1. Ashcroft, F. M., D. E. Harrison, and S. J. H. Ashcroft. 1984. Glucose induces closure of single potassium channels in isolated rat pancreatic β-cells. *Nature (Lond.).* 312:446–448.
2. Atwater, I., and P. M. Beigelman. 1976. Dynamic characteristics of electrical activity in pancreatic β-cells. Effects of calcium and magnesium. *J. Physiol. (Paris).* 72:769–786.
3. Atwater, I., C. M. Dawson, B. Ribalet, and E. Rojas. 1979. Potassium permeability activated by intracellular calcium ion concentration in the pancreatic β-cell. *J. Physiol. (Lond.).* 288:575–588.
4. Atwater, I., C. M. Dawson, A. Scott, G. Eddlestone, and E. Rojas. 1980. The nature of the oscillatory behavior in electrical activity for pancreatic β-cells. *In* Biochemistry and Biophysics of the Pancreatic β-cell. Georg Thieme Verlag, New York. 100–107.
5. Atwater, I., B. Ribalet, and E. Rojas. 1979. Mouse pancreatic β-cells: tetraethylammonium blockage of the potassium permeability increase induced by depolarization. *J. Physiol. (Lond.).* 288:561–574.
6. Atwater, I., E. Rojas, and A. Scott. 1979. Simultaneous measurements of insulin release and electrical activity from single microdissected mouse islets of Langerhans. *J. Physiol. (Lond.).* 291:57P.
7. Beigelman, P. M., B. Ribalet, and I. Atwater. 1977. Electrical activity of mouse pancreatic β-cells. II. Effects of glucose and arginine. *J. Physiol. (Paris).* 73:201–217.
8. Chay, T. R. 1985. Chaos in a three-variable model of an excitable cell. *Physica.* D16:233–242.
9. Chay, T. R. 1985. Glucose response to bursting-spiking pancreatic β-cells by a barrier kinetic model. *Biol. Cybern.* 52:339–349.
10. Chay, T. R. 1986. On the effect of the intracellular calcium-sensitive K^+ channel in the bursting pancreatic β-cell. *Biophys. J.* 50:765–777.

11. Chay, T. R., and J. Keizer. 1983. Minimal model for membrane oscillations in the pancreatic β-cell. *Biophys. J.* 42:181–190.
12. Chay, T. R., and J. Keizer. 1985. Theory of the effect of extracellular potassium on oscillations in the pancreatic β-cell. *Biophys. J.* 48:815–827.
13. Chay, T. R., and J. Rinzel. 1985. Bursting, beating, and chaos in an excitable membrane model. *Biophys. J.* 47:357–366.
14. Cook, D. L., and C. N. Hales. 1984. Intracellular ATP directly blocks K^+ channels in pancreatic β-cells. *Nature (Lond.).* 311:271–273.
15. Cook, D. L., M. Ikeuchi, and W. Y. Fujimoto. 1984. Lowering of pH_i inhibits Ca^{2+}-activated K^+ channels in pancreatic β-cells. *Nature (Lond.).* 311:269–271.
16. Cunningham, E. B. 1978. Biochemistry: Mechanisms of Metabolism. McGraw-Hill Book Co., New York.
17. Dunne, M. J., I. Findlay, and O. H. Petersen. 1984. Patch-clamp study of voltage- and Ca^{2+}-activated K^+ channels in isolated rat pancreatic islet cells. *J. Physiol (Lond.).* 354:44P
18. Findlay, I., M. J. Dunne, and O. H. Petersen. 1985. High-conductance K^+ channel in pancreatic islet cells can be activated and inactivated by internal calcium. *J. Membr. Biol.* 83:169–175.
19. Findlay, I., M. J. Dunne, S. Ulrich, C. B. Wollheim, and O. H. Petersen. 1985. Quinine inhibits Ca^{2+}-independent K^+ channels whereas tetraethylammonium inhibits Ca^{2+}-activated K^+ channels in insulin-secreting cells. *FEBS (Fed. Eur. Biochem. Soc.) Lett.* 185(1):4–8
20. Henquin, J. C. 1978. D-glucose inhibits potassium efflux from pancreatic islet cells. *Nature (Lond.).* 271:271–273.
21. Henquin, J. C. 1977. Tetraethylammonium potentiation of insulin and inhibition of rubidium efflux in pancreatic islets. *Biochem. Biophys. Res. Commun.* 77:551–556.
22. Henquin, J. C. 1980. The potassium permeability of pancreatic islet cells: mechanisms of control and influence on insulin release. *In* Biochemistry and Biophysics of the Pancreatic β-Cell. Georg Thieme Verlag, New York. 66–73.
23. Henquin, J. C., and A. E. Lambert. 1975. Cobalt inhibition of insulin secretion and calcium uptake by isolated rat islets. *Am. J. Physiol.* 228(6):1669–1667.
24. Herchuelz, A., and W. J. Malaisse. 1980. The dual regulation of calcium efflux from pancreatic islets. *In* Biochemistry and Biophysics of the Pancreatic β-Cell. Georg Thieme Verlag, New York. 116–121.
25. Hindmarsh, A. C. 1974. Ordinary differential equations systems solver. Technical Report UCID-30001, Lawrence Livermore Laboratory, Livermore, CA.
26. Hodgkin, A., and A. F. Huxley. 1952. A quantitative description of membrane current and its application to conduction and excitation in nerve. *J. Physiol (Lond.).* 117:500–544.
27. Lindstrom, P., and J. Sehlin. 1984. Effect of glucose on the intracellular pH of pancreatic islet cells. *Biochem. J.* 218:887–892.
28. Meech, R. W., and R. C. Thomas. 1980. Effect of measured calcium chloride injections on the membrane potential and internal pH of snail neurones. *J. Physiol (Lond.).* 298:111–129.
29. Meissner, H. P., and M. Preissler. 1979. Glucose-induced changes of the membrane potential of pancreatic β-cells: their significance for the regulation of insulin release. *In* Treatment of Early Diabetes. R. A. Camerini-Davalos and B. Hanover, editors. Plenum Publishing Corp., New York. 97–107.
30. Meissner, H. P., and H. Schmelz. 1974. Membrane potential of beta-cells in pancreatic islets. *Pfluegers Arch. Eur. J. Physiol.* 351:195–206.
31. Pace, C. S. 1984. Role of pH as a transduction device in triggering electrical and secretory responses in islet B cells. *Fed. Proc.* 43(9):2379–2384.
32. Petersen, O. H., and Y. Maruyama. 1984. Calcium-activated potassium channels and their role in secretion. *Nature (Lond.).* 307:693–696.
33. Prentki, M., and C. B. Wollheim. 1984. Cytosolic free Ca^{2+} in insulin secreting cells and its regulation by isolated organelles. *Experientia.* 40:1052–1060.
34. Rorsman, P., H. Abrahamsson, E. Gylfe, and Bo Hellman. 1984. Dual effects of glucose on the cytosolic Ca^{2+} activity of mouse pancreatic β-cells. *FEBS (Fed. Eur. Biochem. Soc.) Lett.* 170(1):196–200.
35. Satin, L. S., and D. L. Cook. 1985. Voltage-gated Ca^{2+} current in pancreatic B-cells. *Pfluegers Arch. Eur. J. Physiol.* 404:385–387.
36. Scott, A. M., I. Atwater, and E. Rojas. 1981. A method for the simultaneous measurement of insulin release and B cell membrane potential in single mouse islets of Langerhans. *Diabetologia.* 21:470–475.
37. Wollheim, C. B., and G. W. G. Sharp. 1981. Regulation of insulin release by calcium. *Physiol. Rev.* 61(4):914–972.
38. Wollheim, C. B., and T. Pozzan. 1984. Correlation between cytosolic free Ca^{2+} and insulin release in an insulin-secreting cell line. *J. Biol. Chem.* 259:2262–2267.